ISSN 1052-6188, Journal of Machinery Manufacture and Reliability, 2017, Vol. 46, No. 2, pp. 168–174. © Allerton Press, Inc., 2017.
Original Russian Text © E.A. Klyatskina, M.D. Sal'vador, E.F. Segobiya, P. Karpin'o, A. Borrel', E. Sanches, V.V. Stolyarov, 2017, published in Problemy Mashinostroeniya i Nadezhnosti Mashin, 2017, No. 2, pp. 97–105.

NEW TECHNOLOGIES IN MANUFACTURING

Investigation of Deformation Behavior and Fracture of Ceramic Coatings by the Acoustic Emission Method

E. A. Klyatskina, M. D. Sal'vador[a], E. F. Segobiya[a], P. Karpin'o[a], A. Borrel'[a], E. Sanches[b], and V. V. Stolyarov[c, d]

[a] *Materials Technological Institute, Polytechnic University, Valencia, Spain*
[b] *Institute of Ceramic Technology, Jaume I University, Castelló de la Plana, Spain*
[c] *Mechanical Engineering Research Institute, Russian Academy of Sciences, Moscow, Russia*
[d] *National Research Nuclear University MEPhI, Moscow, Russia*

Received September 12, 2016

Abstract—The use of protective coatings on components of machines and mechanisms provides the greatest economic benefit at the lowest additional cost. Plasma spraying is one of the most productive, technologically advanced, and efficient methods of producing these coatings. The results of investigations of structures, mechanical properties, and fracture surfaces of ceramic wear resistant coatings produced by plasma spraying have been presented.

DOI: 10.3103/S1052618817020078

Intensive economic development and its efficiency increase are largely determined by the use of new technological processes. Advanced technologies based on major basic studies (laser, plasma, and powder metallurgy, self-propagating high-temperature synthesis, etc.) make a significant contribution to the development of special engineering.

It is impossible to produce machinery and equipment for operation under extreme conditions (large dynamic loads, aggressive media, erosive and abrasive wear, etc.) is impossible without using special coatings. Special coatings are used to save high-alloy materials and to harden surfaces in order to give them special properties, such as protection from exposure to high temperatures, thermal erosion wear, neutron fluxes and radio emissions, abrasive wear, and the restoration of the geometric dimensions of the surface of worn-out details [12].

The protective coating material is determined based on the conditions of its use. In the case of oxide-containing materials (ZrO_2–Y_2O_3 and Al_2O_3–TiO_2), one of the main limiting factors of their use is low plasticity, as a result of which they fracture (due to cracking, delamination, or loss of material) [3].

Coating strength is an important characteristic that determines the performance of products. Low strength can be caused by the physical nature of the coating structure consisting of separate relatively weakly bound particles and layers, porosities, and lack of volume coupling during the formation. Cohesive and adhesive strengths of welding regions is low as a consequence of defects in their structure. In addition, low adhesive strength is often caused by the difference in types of connections between the base material and the coating.

In view of the above-mentioned, a need arises for standard special tests for the evaluation of the mechanical properties of ceramic coatings. One such method would be to use acoustic emission together with bending tests to investigate the phenomenon of the emergence of sound waves during the deformation of solids. Acoustic emissions are associated with the radiation of stress waves generated in the solid during deformation as a result of discrete dynamic processes, such as the occurrence of macro- and microcracks during operation, which, as is known, are accompanied by the release of energy [4, 5]. This method makes it possible to investigate the mechanisms of the fracture of materials, namely, the high sensitivity of the acoustic emission method makes it possible to determine the defectology type, which includes the size and number of defects, the amount of adhesion, and the cohesion force, as well as the effect of the location of defects with respect to the applied stress [6]. Different microdefects in the sample structure generated during deposition have no significant effect on the mechanical properties; however, as stress concentrators, they can initiate fracture.

Table 1.

Material	$ZrO_2:Y_2O_3$			$Al_2O_3:TiO_2$		
Notation	**mYSZ**	**nYSZ**	**dYSZ**	**mAlTi**	**nAlTi**	**dAlTi**
Provider*	SM	IAM	MCh	SM	IAM	
Brand	M204NS	NS4007	S041981	M130	S2613S	S2613P
Component contents, %	92 : 8	93 : 7	93 : 7	87 : 13		
Particle size (nm)	11–125	50–500	10–15	30–50	20–60	15-40
Agglomerate size (μm)	–	–	10–30	–	–	13–120

SM: Sulzer Metco, IAM: Inframat Advanced Materials, MCh: MEL Chemicals, *M: Metco, *N: Nanox.

The purpose of this paper is to investigate the possibility of using the acoustic emission method to estimate the fracture resistance of ceramic coatings obtained by plasma spraying.

MATERIAL, OBJECTS, AND METHODS OF INVESTIGATION

Two types of ceramic coatings (based on the yttria-stabilized zirconia and the mix of corundum with titanium oxide) were investigated. For each material, three types of powder for deposition with different granulometric compositions were selected, i.e., micro- (m), nano- (n), and nano-agglomerate (d). The fraction size and specifications of powders are given in Table 1. The d-fraction powder (nano-agglomerate) was obtained based on the nanopowder after microencapsulation by spray drying of particles with a size of 50 nm in agglomerates of dozens of microns in order to improve the technological characteristics of the powder for deposition.

Rectangular plates with a thickness of 2 mm made of AISI 316L stainless steel were used as a substrate for the coating. The surfaces of all of the samples was prepared for sandblasting deposition using silicon carbide particles up to the surface roughness of 1.69 μm. In order to improve the adhesion to the substrate, the intermediate layer of AMDRY 997 nickel alloy was applied to the prepared surface. The thickness of the investigated coatings was about 200 μm. The structure and distribution of elements on the coating samples were examined.

The following structural analysis methods were used.

Optical microscopy using a Nikon LV 100 optical microscope with Nis elements 8 software for metallographic control of the thickness of structural components of plasma coatings.

Scanning electron microscopy (in different modes) on the JSM 6300 microscope with an XMax20 X-ray analyzer made by Oxford Instruments for element-by-element composition determination (DRX). The porosity of the coating was measured on thin coating sections using Visilog V5.3 image analysis software according to the ASTM E 2109-01 standard. Bending tests were carried out by a four-point bending scheme. An Instron 4202 universal test machine was used. Samples were set so that the coating was on the support plate in the lower grip of the universal machine. The length and width of samples were 49 ± 1 mm and 8.0 ± 0.5 mm, respectively. The length ratio between the support plates and the sample was 16 : 1. The ratio of the distance between the two load and support rollers was 1 : 2. Acoustic emission signals induced in the loading process were analyzed by the acoustic emission complex Vallen AMSY-5. Acoustic emission data were recorded during bending tests. The frequency range of used piezoelectric sensors was 10–150 kHz (the preamplifier 34 dB and the detection zone 40 dB). Because of the features of the sample geometry, two of piezoelectric sensors were mounted on the supports symmetrically with respect to the tested sample (due to its size and configuration), which differed from the circuit used by other authors [7–9], where the piezoelectric sensor was mounted directly on the sample.

RESULTS AND DISCUSSION

Corundum–titanium oxide coatings. Coatings obtained from the powders of three different granulometric compositions have a layered anisotropic microstructure parallel to the coated surface. In Fig. 1, it is possible to distinguish the layers of the solid solution of titanium oxide and aluminum oxide. According to energy-dispersive analysis, light-gray layers are enriched in titanium oxide (zone 1). Light areas (zone 2 in Fig. 1) correspond to the underlayer material covered during the spraying of the base coating layer. Microcracks are caused by high thermal stresses during the sample rapid cooling.

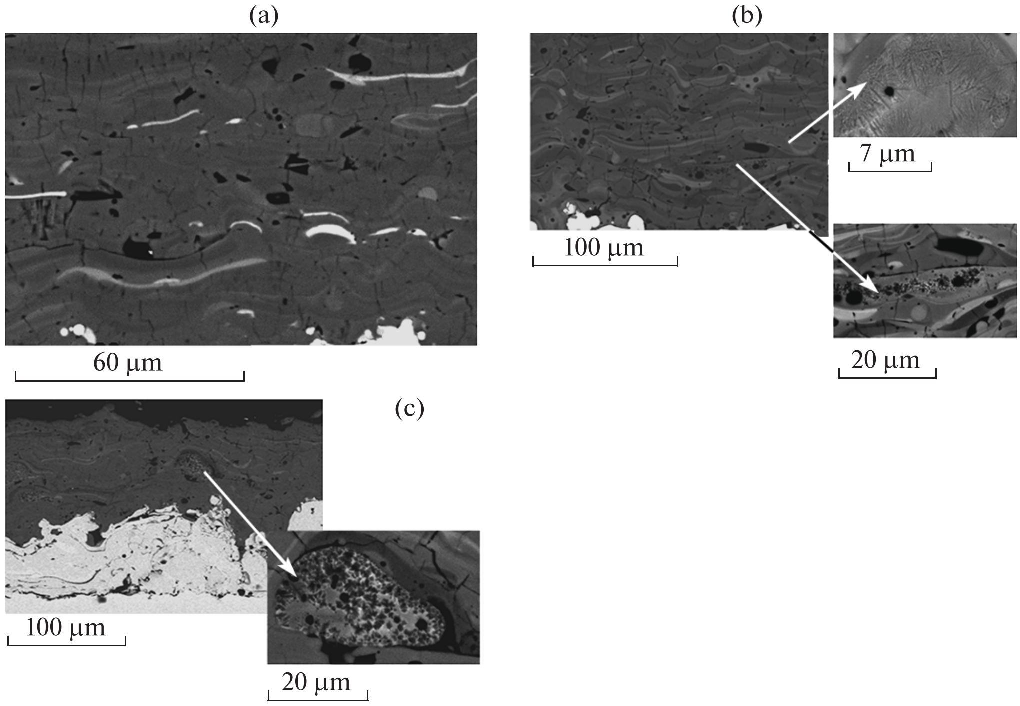

Fig. 1. Section microstructure of AlTi coatings (backscattered electron mode) made of (a) mAlTi micromaterial, (b) nanomaterial nAlTi, and (c) nanoagglomerate dAlTi.@Key:мкм → μm.

Samples obtained from nano (n) and nanoagglomerate (d) powders have duplex structure (Figs. 1b and 1c). They include flattened layers consisting of unmelted partially melted particles of the initial powder. The layered microstructure of the coating on the ~~thin~~ section is determined by different shades of gray, which corresponds to chemical elements with different atomic weight. This is due to the presence of zirconium oxide and yttrium oxide additives in the initial material. Partially melted fragments of the initial material were also detected.

Unmelted particles of the initial material of two morphology types were detected in the ~~microsection~~ of the dAITi coating (Fig. 1c) obtained from the nanoagglomerated powder.

Partially melted particles found in this surface are larger than those available in the nanocoating (nAITi). Microcracks and mi ores around partially melted and unmelted particles of the initial material were detected on the ~~thin~~ section of the coating sample obtained from the nanoagglomerate powder. This type of microstructure was also described in [4, 10, 11]. The porosity of the coating was measured. For m, n, and d materials, it was 6.1%, 5.0%, and 4.6%, respectively.

In order to obtain source information on the initiation and developme cracking and the coating fracture during the bending test, diagrams ~~of the dependence~~ of the amplitude nd number of signals on the time were constructed and synchronized with the loading graph (Fig. 2). Each point corresponds to the number of signals (or their amplitude) detected during the sample bending. Each signal with an amplitude above 40 dB means that the coating is subjected to some microdefect under the stresses that act on it [11].

According to its nature, the ceramic coating fracture is fragile. In this case, it is quite difficult to determine three typical fracture zones and their corresponding stresses [12].

Based on the fract theory proposed by Lin in [13], it was possible to separate individual coating deformation steps. Th stages characteristic of a particular fracture stress were identified. The analysis of the resulting diagrams made it possible to determine these stresses for three types of Al_2O_3–TiO_2 coatings. The results are given in Table 2.

The characteristic stress of the microfracture of σ_1 coatings that correspond to the occurrence of microcracks is in the straight-line area on the loading diagram. At this time, acoustic emission detects a small number of signals with amplitudes that do not exceed 60 dB. The stress σ_2 is recorded at the place of the maximum accumulation of acoustic emission signals. The stress σ_3 corresponds to the catastrophic coating failure and is in the nonlinear region of high stresses and deflection (Fig. 2).

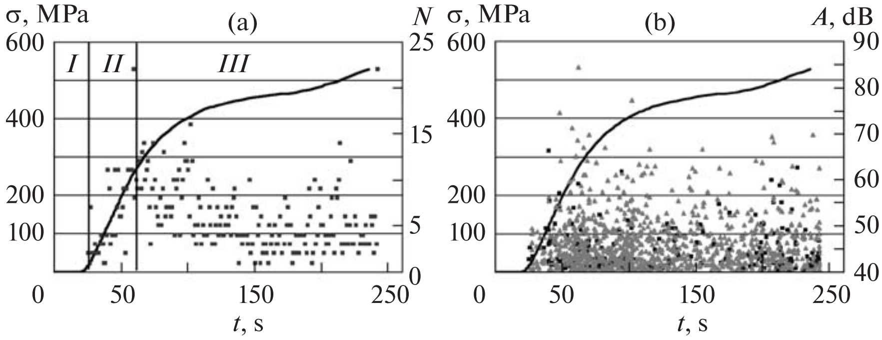

Fig. 2. Loading diagrams of the mAlTi coating synchronized with the (a) number and (b) amplitude of acoustic emission signals.

The formation of microcracks was first observed in nano- and nanoagglomerated coatings than in micrometer coatings. The microstructure of these coatings includes duplex elements that contain partially melted particles within the flattened material matrix. Microcracks in the microstructure (caused by the thermal stress) and discontinuities and porosity between the matrix and partially melted particles cause the appearance of microcracks at low stresses during the test.

The complete destruction of the micrometer coating occurs at lower stresses. This is due to the differences between the fracture mechanism of this type of coating and the mechanism inherent in nanocoatings [14, 15].

In micrometric coatings, cracks form along the boundaries of flattened layers of the hardened coating. In nanostructured coatings, a crack does not extend by the flattened layer boundary, but it expands in the nanostructured material, which was created by spraying the coating up to larger size particles formed from the initial partially melted powder. Any stress applied to the nanostructured coating is compensated for by the formation of microcracks perpendicular to the coating surface. In turn, these microcracks are inhibited by the microstructure nanostructured components before they go through the entire thickness of the coating or connect with other microcracks. The differences in microstructure explain why on the acoustic emission graph there are fewer signals for micrometer coatings than for nanometric and nanostructured ~~compact~~ coatings.

Yttria-stabilized zirconia (YSZ) coatings. Ceramic coatings based on zirconium oxide were obtained from industrial micrometric and nanometric powders and from the agglomerated nanostructured powder produced from the suspension.

Industrial nanoparticle suspension was atomized by spray d[illegible]g. As a result, the material in the form of agglomerates was obtained. The morphology, size, and yie[illegible]tisfy plasma spraying conditions. This material in the form of agglomerates was subjected to thermal [illegible]ects in order to achieve the desired sealing/sintering level.

Figure 3 shows ~~photographs of~~ microsections of the coating with numerous microdefects.

Microdefects are positive for the use of these coatings for heat protection, but they have a negative effect on the mechanical properties of the coatings. A significant thermal conductivity reduction associated with porosity and cracks parallel to the substrate surface and the coating was proved [16]. The type, size, orientation in space, and contents of pores directly affect the thermal conductivity. The highest porosity level was detected in the micrometer coating was 22.5%, whereas ~~for~~ nanometer and nanoagglomerated coatings the porosity was 13.5%. As in ~~the~~ case of coatings of aluminum oxide with titanium oxide, the microstructure of nanometric and nanoagglomerated coatings contains unmelted particles of the initial material, which could stop or redirect crack growth during the bending test.

Table 2.

Stress, MPa	**nAlTi**	**mAlTi**	**dAlTi**
σ_1	10 ± 2	110 ± 7	50 ± 4
σ_2	420 ± 36	250 ± 28	410 ± 12
σ_3	890 ± 39	850 ± 43	910 ± 57

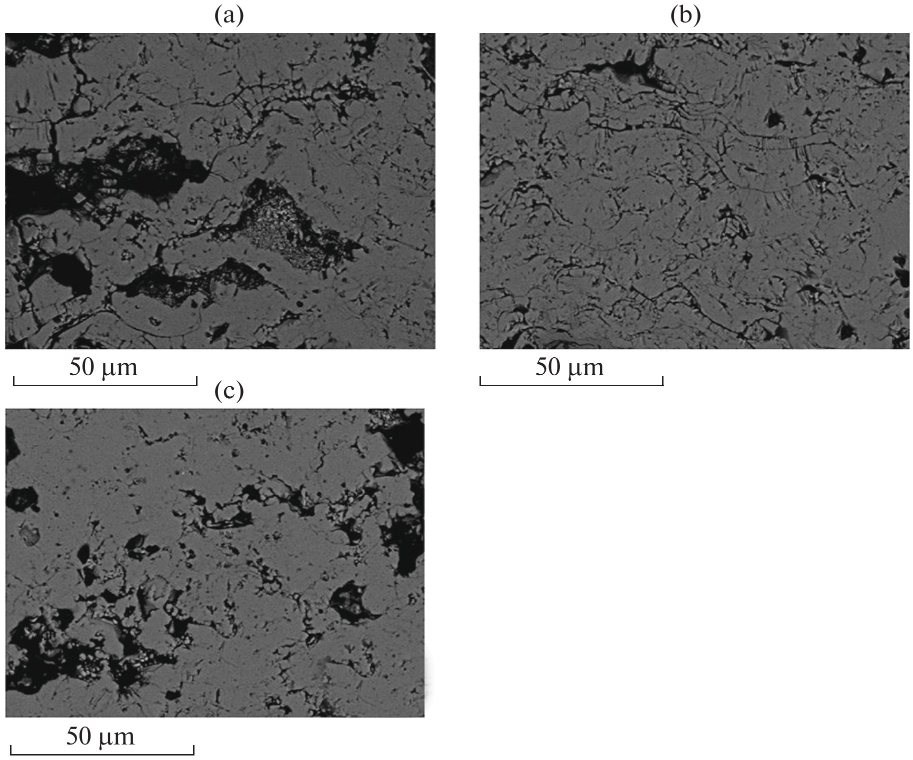

Fig. 3. Section microstructure of YSZ coatings transverse (secondary electron mode): (a) nYSZ, ×200, (b) mYSZ, ×200, and (c) dYSZ, ×200.

Loading diagrams of micro- (*m*), nano- (*n*), and nanoagglomerated (*d*) YSZ coatings are shown in Fig. 4. As in the case of previously described ceramic coatings, YSZ coatings fracture in three steps, i.e., (1) the formation of microcracks, (2) crack growth, and (3) and catastrophic failure. Data obtained using acoustic emissions made it possible to distinguish between these stages and associate them with stresses. Table 3 contains data on the values of fracture stresses for the ZrO_2 coating stabilized by Y_2O_3 in critical areas determined by fracture diagrams and detection of acoustic emission signals. The sample surface state was investigated after mechanical tests.

Unlike Al_2O_3–TiO_2 coatings, cracks were not found on the surface of ZrO_2–Y_2O_3 coating samples. Vertical cracks were only detected on the cross section under an optical microscope (Fig. 5).

It should be noted that the tested samples did not have coating delamination. As a result, it was impossible to determine the stress σ_3 that corresponds to the stage of catastrophic failure for this type of coating. According to the investigations of Wang and Liang in [17, 18], zirconium oxide coatings have a high level of fracture resistance as compared with other ceramic coatings. The largest number of acoustic emission signals (over 25) was detected for nanometric coatings. It should be noted that this coating is the most porous of all the investigated coatings.

The average number of signals (15) was detected for the nanoagglomerated coating (d YSZ). The lowest number of signals was obtained for the m YSZ coating (less than 10 for all of the samples).

The bending behavior of samples can be explained by differences in their microstructures. Samples of nanometric and nanoagglomerated coatings show the highest values of stress σ_2 because of partially melted particles in the microstructure, which, in turn, prevent the growth and propagation of cracks.

Table 3.

Stress, MPa	**n YSZ**	**m YSZ**	**d YSZ**
$\boldsymbol{\sigma_1}$	3 ± 2	8 ± 3	17 ± 2
$\boldsymbol{\sigma_2}$	200 ± 40	180 ± 17	300 ± 20

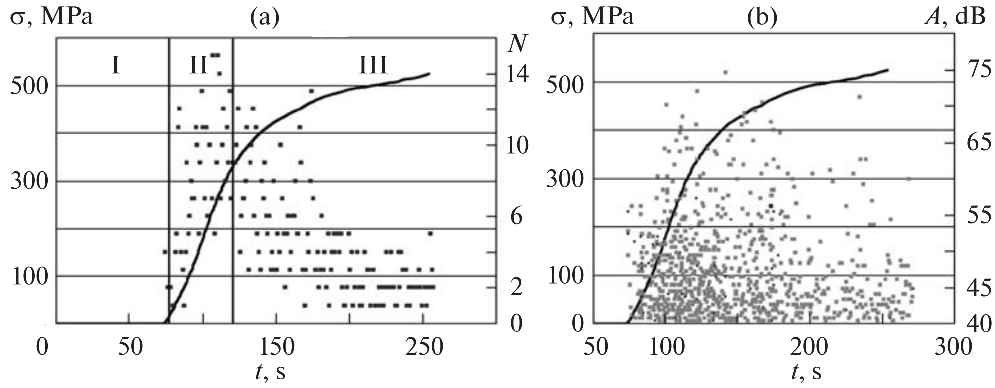

Fig. 4. Loading diagrams of dYSZ coatings synchronized with the number (a) and amplitude (b) of acoustic emission signals.

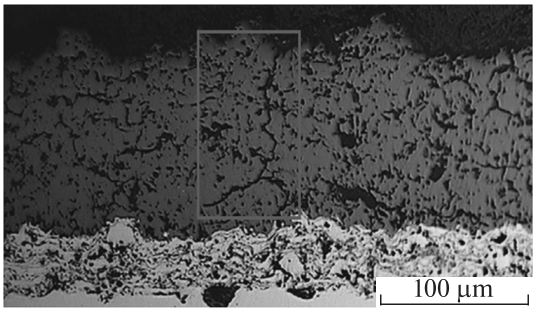

Fig. 5. Section microstructure of dYSZ coating after bending tests, ×250.

Crack formation stress (σ_1) is smaller for yttrium-stabilized zirconium oxide coatings than for the titanium oxide–aluminum oxide coatings because of the higher porosity and a large number of defects in the YSZ coatings.

CONCLUSIONS

It has been established that the major role in the deformation behavior of coatings of both ceramics during bending is played by the microstructure. Two types of microstructure are distinguished for the investigated coatings. The first type is characteristic of micrometer coatings, in which it is represented by anisotropic layers parallel to the contact surface with the substrate.

The second type of microstructure is characteristic of nanometric coatings. This is a duplex structure that consists of alternating layers of partially melted and unmelted grains of the initial powder. The use of the acoustic emission method, along with bending tests, made it possible to establish the mechanism of coating failure, which includes three main stages, i.e., the formation of microcracks between the layers, their growth, and destruction in the form of coating delamination. In the case of micrometer coatings, the fracture occurs at much lower stresses than for nanometric coatings. The microcrack initiation stress is lower for nanometric than micrometer coatings. Micrometric coatings have the highest acoustic emission activity. Coatings based on the yttria-stabilized zirconia showed higher fracture resistance than Al2O3–TiO2 coatings. In these coatings, there is no stripping under maximum sample deflection.

ACKNOWLEDGMENTS

The article was supported by the Ministry of Economy, Industry and Competitiveness of Spain (project no. MAT2015-67586-C3R) and the Regional Government of Valencia (project no. VALiD APOSTD/2014/046).

REFERENCES

1. Cartier, M., *Handbook of Surface Treatments and Coatings. Tribology in Practice Series,* London: Professional Engineering Publishing, 2003.
2. Lesyevskii, L.N., Lezhnev, L.Yu., Lyakhovetskii, M.A., et al., Inorganic solid lubricating coatings for heat engines and power plants, *J. Mach. Manuf. Reliab.,* 2015, vol. 44, no. 5, pp. 455–463.
3. Bhushan, B., *Handbook of Tribology. Materials, Coatings, and Surface Treatments,* New York: McGraw Hill, 1991, pp. 14–68.
4. Bansal, P., Padture, N.P., and Vasiliev, A., Improved interfacial mechanical properties of Al_2O_3–13 wt % TiO_2 plasma-sprayed coatings derived from nanocrystalline powders, *Acta Mater.,* 2003, vol. 51, pp. 2959–2970.
5. Cox, L.C., The four-point bend test as a tool for coating characterization, *Surf. Coat. Technol.,* 1988, vol. 36, pp. 807–815.
6. Dunegan, H.L., Location of leaks in pipes by use of acoustic emission modal ratio techniques, *Met. Eng. Quart.,* 1975, pp. 8–16.
7. Miguel, J.M., Guilemany, J.M., Mellor, B.G., et al., Acoustic emission study on WC-Co thermal sprayed coatings, *Mater. Sci. Eng.,* 2003, vol. 352, pp. 55–63.
8. Dalmas, D., Benmedakhene, S., Richard, C., et al., Caractérisation par émission acoustique de l'adhérence et de l'endommagement d'un revêtement: cas d'un revêtement WC-Co sur acier Chimie, *Chemistry,* 2001, no. 4, pp. 345–350.
9. Roques, A., Browne, M., Thompson, J., et al., Drug delivery systems in cancer therapy, *Biomat.,* 2004, vol. 25, pp. 769–778.
10. Gell, M., Jordan, E.H., Sohn, Y.H., et al., Development and implementation of plasma sprayed nanostructured ceramic coatings, *Surf. Coat. Teclmol.,* 2001, vol. 14, pp. 648–654.
11. Goberman, D., Sohn, Y.H., Shaw, L., et al., Microstructure development of Al_2O_3–13wt.%TiO_2 plasma sprayed coatings derived from nanocrystalline powders, *Acta Mater.,* 2002, vol. 50, pp. 1141–1152.
12. Salvador, M.D., Klyatskina, E., Bonache, V., et al., Estudio por emisión acustica del comportamiento a flexión de recubrimientos WC-Co obtenidos por plasma atmosférico, *Revista Metalurg.,* 2007, vol. 43, pp. 414–423.
13. Lin, C.K., Bernd, C.C., Leigh, S.H., et al., Modelling of elastic constants of plasma spray deposits with ellipsoid-shaped voids, *J. Am. Ceram. Soc.,* 1997, vol. 80, pp. 2382–2394.
14. Kabacoff, L., Opportunities in protection materials science and technology for future army applications, *AMPTIAC Newslett.,* 2002, no. 6, pp. 37–43.
15. Hanshin Choi, C.L. and Kim, H.J., Processing and characterization of alumina/chromium carbide ceramic nanocomposite, *J. Ceram. Processing Res.,* 2002, no. 3, pp. 210–215.
16. Carpio, P., Blochet, Q., Pateyron, B., et al., Correlation of thermal conductivity of suspension plasma sprayed yttria stabilized zirconia coatings with some microstructural effects, *Mater. Lett.,* 2013, vol. 107, pp. 370–373.
17. Wang, W.Q., Sha, C.K., Sun, D.Q., and Gu, X.Y., Preparation and characterization of nanostructured Al_2O_3–13wt.%TiO_2 ceramic coatings by plasma spraying, *Mater. Sci. Eng.,* 2006, vol. 424, pp. 1–5.
18. Liang, B. and Ding, C., Microstructure analyses and thermo-physical properties of nanostructured thermal barrier coatings, *Surf. Coat. Technol.,* 2005, vol. 197, pp. 185–192.

Translated by O. Pismenov

SPELL OK